Quasistationary field of thermal emission and near-field radiometry

A. N. Reznik, V. L. Vaks, and N. V. Yurasova
Institute for Physics of Microstructures, 603950 Nizhny Novgorod, Russia
(Received 26 March 2004; published 4 November 2004)

We provide a theory of radiometry measurements of the quasistationary (near) field of thermal emission from a heated conducting medium. It explains why the Rytov effect, which essentially is a drastic growth of the thermal field energy near the medium surface, cannot be detected experimentally. However, we discovered a measurable near-field effect: the effective depth of formation of the received emission proves to be less than the skin-layer depth, depending on the size of the receiving antenna and its height above the surface. For such measurements highly effective antennas of a small aperture size are necessary. We developed and investigated a variety of microwave antennas whose parameters were fairly suitable for near-field radiometry. The measurements conducted with these antennas yielded experimental evidence of the fact that the quasistationary thermal field really exists. Near-field radiometry opens further opportunities for investigating media. In particular, we demonstrate here a technique for retrieval of the subsurface temperature profile in water with the help of near-field measurements.

DOI: 10.1103/PhysRevE.70.056601 PACS number(s): 41.20.Jb

I. INTRODUCTION

A quasistationary (near) field (QF) of thermal emission from a heated absorbing medium was theoretically predicted to exist by Rytov as early as the 1950s [1] (see also [2]). The features of such a field include primarily the absence of energy flux and, second, a fast decrease in the energy spectral density farther from the radiating medium surface. At the same time, near the surface the QF energy increases sharply to values far exceeding the energy of the wave field. It is by this property that the authors in [1,2] suggested identifying the quasistationary field in direct radiometry measurements. Later, the Rytov effect was considered in a number of theoretical studies [3,4], yet no evidence of QF presence has been found so far by measurements of this effect. We managed to settle this inconsistency through our theoretical investigations. It was shown that a QF increase on the surface cannot in principle be detected with an antenna and radiometer. The conclusions of the developed theory are provided in our work [5] and here we describe the theory in detail. Another important fact ensuing from this theory is that the quasistationary field, after interaction with a receiving antenna, acquires a specific space scale—the effective depth of formation of the received radiation, d_{eff}. This depth depends on the receiving antenna aperture size D and height h above the radiating surface; note that $d_{\mathrm{eff}} < d_{\mathrm{sk}}$, where d_{sk} is the depth of the skin layer. The parameter d_{sk} is the characteristic space scale of the wave field. Then, by stating that $d_{\mathrm{eff}} < d_{\mathrm{sk}}$, one can prove that the QF exists. This near-field effect is now measurable, and the experimental results [5,6] obtained to date provide evidence of the QF. In this work we present additional experimental data as unambiguous proof of the QF existence.

Our theoretical study has shown that the QF can be measured with electrically small antennas (ESA's), which have an aperture size smaller than wavelength: $D \ll \lambda$. The available data on ESA properties in the literature (see, for example, [7]) originally suggested that it is hardly possible to detect a QF by this method. Our own experience of ESA development on the basis of high-temperature superconductors [8–10] led us to the same conclusion. Indeed, the narrow operating frequency bands and low efficiency of ESA's seemed to be inadequate to ensure the sensitivity of radiometry systems that would be up to recording a thermal electromagnetic field. It should be noted, however, that the ESA properties were mostly studied for free-space emitters, whereas for an antenna to receive a QF, it has to be in contact with the medium, i.e., be placed at $h \ll \lambda$. It is obvious that the ESA parameters in the vicinity of a conducting medium will undergo considerable change. The characteristics of our first-developed antenna ($D/\lambda \approx 0.03$), the one we used for detecting the QF in [5,6], turned out quite promising. Our efforts were then directed at further miniaturization and upgrading of the antenna design. This work resulted in a near-field antenna facility showing fairly reasonable characteristics at $D/\lambda \geqslant 0.01$. The experimental investigations reported in this work were carried out with the use of these antennas (their parameters are given below).

Advances in near-field radiometry open up challenging opportunities for temperature diagnostics of media. To determine a subsurface temperature profile $T(z)$ it is essential that radiation be simultaneously received from several different depth levels. Then, by solving the inverse problem, it is possible to retrieve the profile $T(z)$. Until recently this diagnostics relied on measuring only the wave component of a thermal field, so the $T(z)$ retrieval procedure involved the dependence $d_{\mathrm{sk}}(\lambda)$, which required several radiometry systems. Near-field measurements extend the capabilities of such a diagnostics, as they allow for using d_{eff} not only as a function of λ but also as a function of D and h. In particular, it seems an interesting idea to retrieve $T(z)$ from measurements taken for one fixed wavelength, which is no doubt a simpler task than multiwave measurements in terms of the measuring system design. The scope of practical applications for subsurface radiothermometry techniques is fairly wide, ranging from medical and biological studies [11–13] to probing of water [14] and soils [15].

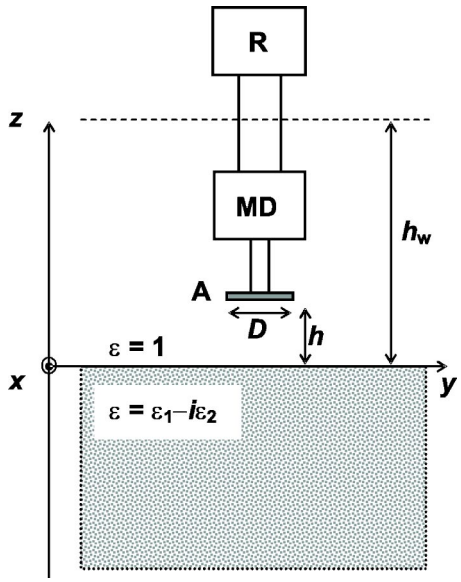

FIG. 1. Scheme of the near-field measurements: A, antenna aperture; R, radiometer; MD, matching device.

This work contains a detailed analysis of the above issues, specifically, the QF measurement theory; the near-field antenna parameters; results of the experimental studies on the QF; and the prospects for near-field radiothermometry.

II. THEORY OF THE QUASISTATIONARY THERMAL FIELD MEASUREMENT

Unlike the theory developed by Rytov [1,2], we here consider the interaction between the thermal emission of a half space and a measuring system comprising an antenna, matching circuit, and radiometer (Fig. 1). The aperture size D of the antenna and its height h above the surface are arbitrary values. The antenna is assumed to be in perfect match with the radiometer input circuit, i.e., at operating frequency f_0 the reflectivity from the matching device $R=0$. In addition, the antenna efficiency is taken to be 1, which corresponds to the absence of Ohmic losses in the emitter and matching device materials. Thermal emission is generated by macroscopic fluctuation currents $\mathbf{j}(\mathbf{r})$ flowing in the absorbing half space with permittivity $\varepsilon=\varepsilon_1-i\varepsilon_2$, which are set, according to [2], by the correlation function

$$\langle j_i(\mathbf{r},z)j_k^*(\mathbf{r}_1,z_1)\rangle = \frac{\omega\Theta(z)}{4\pi^2}\varepsilon_2\delta_{ik}\delta(\mathbf{r}-\mathbf{r}_1)\delta(z-z_1), \quad (1)$$

where $\Theta(z)=(\hbar\omega/2)\coth[\hbar\omega/2\kappa T(z)]$ is the Planck function. Solution of the electrodynamical problem on the radiometer-measured emission power P, which is provided in the Appendix, yielded the following result:

$$P = P_W + P_Q = \frac{1}{2\pi}\left[\int_{-\infty}^{0} dz\Theta(z)[K_W(z,D,h)+K_Q(z,D,h)]\right], \quad (2)$$

where $P_{W,Q}$ denote the contributions made by the wave and the quasistationary components, respectively, to the total power P. The functions $K_{W,Q}$ are described by the formulas (A13) and (A16), in which the integration domain for K_W is $\kappa\leqslant k_0$, and for $K_Q-\kappa>k_0$. Moreover, according to Eq. (A16), $\int_{-\infty}^{0}dz[K_W(z,D,h)+K_Q(z,D,h)]=1$.

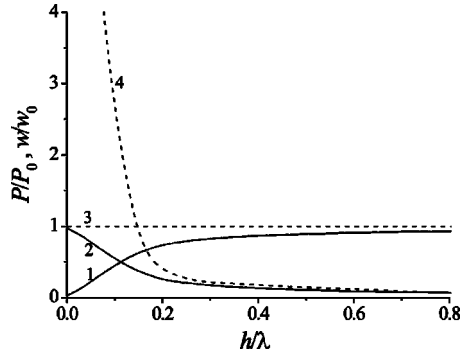

FIG. 2. Normalized power of the wave P_W (curve 1) and the quasistationary P_Q (curve 2) thermal fields as functions of the antenna height h for $D/\lambda=0.1$. Dashed lines, thermal energy density w/w_0 calculated according to [1,2] for the wave (curve 3) and the quasistationary (curve 4) fields.

It follows from Eq. (2) that for a uniformly heated medium $\Theta(z)=\Theta=\text{const}$ the received radiation power is constant, being determined by the Planck intensity of the equilibrium thermal emission $J_0=\Theta/(2\pi\lambda^2)$:

$$P = \frac{\Theta}{2\pi} = \lambda^2 J_0 = P_0, \quad (3)$$

where the power P is independent of the receiving antenna size, the position above the surface, as well as of the dielectric properties of the emitting medium. Thus, a practically measurable parameter is the power P. Due to emission–antenna interaction it features a completely different dependence on h as compared to the energy density w, obtained in [1,2] irrespective of the measuring system. The difference between the dependence $P=P_W(h)+P_Q(h)$, obtained in our study, and the function $w(h)$ from the Rytov theory is seen in Fig. 2. Calculations of the functions $P_{W,Q}(h)$ were performed by formula (2) taking into account Eqs. (A13) and (A16), whereas $w(h)$ was calculated by Eq. (A19) for a medium with permittivity $\varepsilon=76-3i$ (fresh water at $T=20\,^\circ$C, $\lambda=30$ cm). The field distribution over the receiving antenna aperture was approximated by the function $E_a(r)=E_0\exp(-4r^2/D^2)$. The function $w(h)$ in Fig. 2 is normalized to the wave field energy $w_0=w(h\to\infty)$. The energy $w(h)$ also consists of two components, i.e., $w=w_W+w_Q$. In contrast to the obtained dependence $P_W(h)$, the energy $w_w=w_0$ is constant for all values of h. On the other hand, in accordance with the Rytov theory, the energy w_Q depends on h, and for emission sources of the kind (1) it was found that $w(h)\to\infty$ at $h\to 0$. By our theory, the antenna transforms a part of the nonpropagating QF energy into a waveguide mode that features an energy flux. However, the antenna transfer function constrains the divergence of the QF energy at $h=0$. The effect produced by a receiving antenna is thus reduced to redistribution of energy between the wave, P_W, and the quasistationary, P_Q, components in the total power $P=P_0=\text{const}$, re-

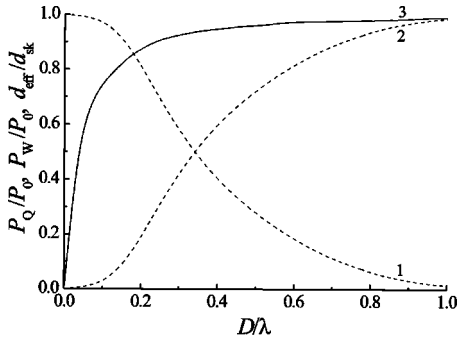

FIG. 3. Normalized power of the quasistationary P_Q (curve 1) and the wave P_W (curve 2) thermal fields as functions of the antenna size D at $h=0$. Curve 3 shows the effective depth of thermal field formation $d_{\mathrm{eff}}/d_{\mathrm{sk}}$.

ceived by the radiometer. In accordance with Eq. (2), although the QF does not cause P to grow above P_0, it also contributes to the received signal along with the wave field. In particular, it is readily seen from Fig. 2 that the partial contribution of the QF in P_0 for electrically small antennas ($D/\lambda \ll 1$) increases closer to the surface and becomes a dominant factor in some height range $h \ll \lambda$. A similar behavior is exhibited by the dependencies $P_{W,Q}(D)$ at $h=0$ in Fig. 3. For antenna apertures $D \ll \lambda$ the P_Q contribution in P dominates too. This led us to the conclusion that the QF effect on the radiometer-received power is strongest when $D/\lambda \ll 1$ and $h/\lambda \ll 1$ simultaneously.

It should be noted that the total received power equals P_0 even at $D \to 0$, just as in the entire range of D variation. This paradox follows from the assumption that the antenna efficiency η is equal to 1 regardless of the antenna size. In other words, we suggested the possibility of transferring the total energy of an auxiliary wave to the absorbing medium through an antenna of an arbitrary small size (see the Appendix). This cannot be achieved in reality because of the inevitable decrease in η with the smaller electrical size of the antenna, D/λ. More details on this problem are provided in the next section.

The result (3) accounts for the fact that the Rytov effect (shown in Fig. 2 as an infinite growth of the energy spectral density w at $h \to 0$) is beyond experimental observation, i.e., it cannot in principle be used for detecting a QF by radiometry measurements.

The fact that the thermal power at $\Theta = \mathrm{const}$ is independent of the antenna position and size does not suggest that there are no detectable effects of the QF. As shown above, it may greatly affect the signal to be measured. In particular, the QF is responsible for the appearance of a new space scale d_{eff} which is basically the effective depth of formation of the received radiation. Let it be defined as

$$d_{\mathrm{eff}} = \left| \int_{-\infty}^{0} dz z K(z) \right|, \tag{4}$$

where $K(z,D,h) = K_W(z,D,h) + K_Q(z,D,h)$ in Eq. (2). According to the calculations shown in Fig. 3, given a strong influence of the QF at $D/\lambda \ll 1$, we have $d_{\mathrm{eff}}(D) < d_{\mathrm{sk}} = 1/(2k_0 \,\mathrm{Im}\sqrt{\varepsilon})$, with d_{eff} tending to zero at $D \to 0$. Most vividly, this near-field effect shows up in conducting media for which $|\varepsilon| \gg 1$ (water, biological tissues, metals, etc.). The skin-layer depth d_{sk} in such media is the characteristic scale of the wave field formation, as is clearly seen from Fig. 3. Therefore, by stating the fact that $d_{\mathrm{eff}} < d_{\mathrm{sk}}$ we provide evidence of the presence of a near-field component in thermal radiation. The physical interpretation of this effect is given in [5,6], while below we discuss the possibility of its experimental registration.

III. NEAR-FIELD ANTENNAS

To ensure effective receiving of thermal radiation from the medium under study it is essential that the radiometer antenna meet certain requirements. We consider these using the expression for the equivalent temperature of the received power (antenna temperature),[1] if the receiving antenna is not ideal:

$$T_a = (1-R)[\eta T_b + (1-\eta) T_m] + R T_n. \tag{5}$$

Here, T_b is the radio brightness temperature of the recorded thermal field of the medium, T_m is the temperature of the antenna material, T_n is the equivalent temperature of the radiometer noise, R is the antenna reflectivity, and η is the antenna efficiency. It is seen from formula (5) that poor matching ($R \neq 0$) and low efficiency ($\eta < 1$) of the antenna reduce the detector sensitivity to temperature T_b which in Eq. (5) is exactly the parameter to be measured, as it alone carries the information about the radiation from the medium in question.

As shown above, the detection of the QF takes electrically small antennas with $D/\lambda \ll 1$. It is known [7] that the matching devices for such antennas have a high Q factor, i.e., they provide a good matching only within a rather narrow frequency band. At the same time, in order to secure a high S/N ratio the working frequency band of the radiometer has to be made as wide as possible. It should be expected that this discrepancy will result in a lower T_b sensitivity of the device. To quantitatively account for this fact, the coefficient R in Eq. (5) should be understood as the antenna reflectivity averaged over the radiometer frequency band. Another important parameter, which is the efficiency η, describes Ohmic losses in the antenna. Typically, the ESA's feature low efficiency. The major contributing factor to this is the losses in the matching circuits, which can also be explained by the high Q of such antennas [7,8]. A decrease in the electrical size of the ESA is often accompanied by simultaneous narrowing of the frequency band and degrading of the efficiency. It is obvious that, starting at some low value of D/λ, it will become impossible to measure thermal fields of the medium in question due to a drop in the sensitivity of the receiving system to T_b in accordance with Eq. (5).

Therefore, the problem of feasibility of QF research using the above technique calls for investigation into the properties

[1]The antenna temperature is related to the radiation power measured, P, as $T_a = 2\pi P/\kappa$ with the condition $\hbar\omega \ll 2\kappa T$, which is generally met in the radio frequency range.

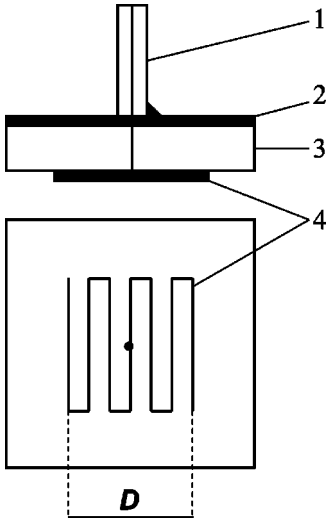

FIG. 4. Schematic diagram of near-field antennas: 1, coaxial cable; 2, background; 3, dielectric substrate; 4, aperture.

of ESA's when they are in contact with the radiating medium. The fact is that earlier investigations of ESA's have mostly been focused on antennas that radiate into free space [7–10]. The dielectric properties of the conducting medium in contact with the antenna aperture will no doubt affect the ESA characteristics. Our earlier study of such ESA's ($D/\lambda \approx 0.03$) is reported in [16]. The same kind of antenna was used in our earlier work for detecting a thermal QF [5,6], where we also provide the key characteristics for this antenna. The fairly high efficiency ($\eta \approx 0.85$) obtained therein suggests that, even if the electrical sizes of the ESA's are decreased further, $D/\lambda < 0.03$, the antenna efficiency will still remain adequate for radiometry measurements of thermal fields. Reducing D/λ is critical because the near-field effect shows up best exactly at extremely low values of D/λ. As seen from the calculations in Fig. 3, an abrupt drop in d_{eff} occurs in the range $D/\lambda < 0.03$, where $d_{\text{eff}}/d_{\text{sk}} < 0.5$.

Research into the quasistationary field was carried out with a specially developed facility that involves three receiving antennas varying in the aperture size D and operating at a wavelength $\lambda \approx 31$ cm. Either antenna was designed as a microstrip resonator whose scattering field provided a link with the medium under study. Matching of the antennas at the radiometer working frequency $f=970$ MHz was ensured by adjusting the length of the arms between the open ends and the connection point, as shown in Fig. 4.

A distinctive feature of the contact antennas is the dependence of input impedance Z_{in} on height h above the emitting surface. Therefore, the best matching at a specified working frequency f_0 and the same geometry of antenna can be achieved only for one certain value of h. In our facility all antennas were matched to the radiometer while being in close contact with the test medium surface (water), i.e., at $h=0$. The reflectivity spectra $R(f)$ for one of the antennas with $D=20$ mm and different values of h are given in Fig. 5. The same figure shows a normalized amplitude-frequency characteristic of the radiometer, $A(f)[\int_0^{+\infty} dfA(f)=1]$. Note that the maximum of the function $A(f)$ and the minimum of reflectivity $R(f,h=0)$ are at the same frequency $f=f_0$

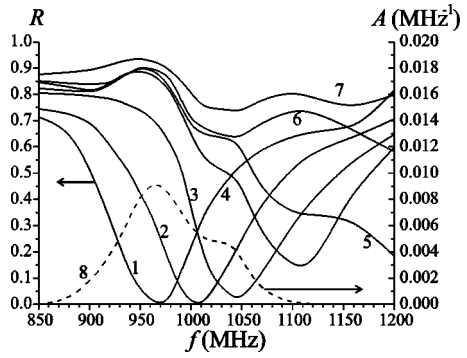

FIG. 5. Antenna reflectivity at various heights h above water. Curve 1 corresponds to $h=0$; 2, $h=1$ mm; 3, $h=1.5$ mm; 4, $h=2$ mm; 5, $h=2.5$ mm; 6, $h=3$ mm; 7, $h=5$ mm; dashed line 8, normalized frequency response of the radiometer.

$=970$ MHz. It is seen from Fig. 5 that an increase in h leads to both a shift of the antenna resonance frequency and an antenna-radiometer mismatch. Figure 6 shows the reflectivity at the radiometer working frequency, $R(f_0,h)$, and also its value averaged over the radiometer frequency band, $\langle R(h)\rangle = \int_0^{+\infty} dfA(f)R(f,h)$. One can see that even at $h>1.5$ mm we had $\langle R\rangle > 0.5$. Note that it is the value of $\langle R\rangle$ that we use as the reflection coefficient R in formula (5).

A very important characteristic of a receiving antenna, which determines the sensitivity of the measuring system to T_b in accordance with Eq. (5) is the efficiency η. We find it from the calibration measurements of the receiver response to emission of uniformly heated water for two different states $T_b=T_1$ and $T_b=T_2$. Then, using Eq. (5), we have

$$\eta(h) = \frac{\delta T/\delta T_b(h)}{1-\langle R(h)\rangle}, \tag{6}$$

where $\delta T_b(h)$ is the fluctuation threshold of sensitivity of the measuring system, and δT is the fluctuation threshold for the case when a matched load ($\langle R\rangle = 0$, $\eta = 1$) is connected to the radiometer input instead of antenna. Naturally, the lower the fluctuation threshold, the higher is the sensitivity of the system. Maximum sensitivity is reached when the radiometer has a matched load connected to it, i.e., $\delta T < \delta T_b$ corresponds to the intrinsic sensitivity of the radiometer. Since the

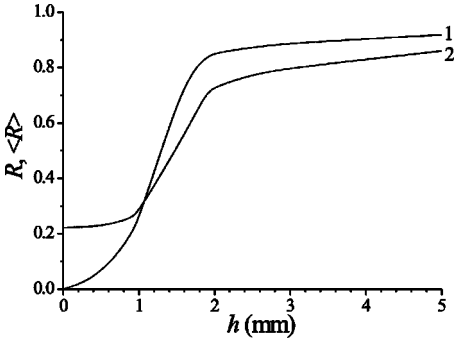

FIG. 6. Reflection coefficient R at resonance frequency (curve 1) and its value averaged over the radiometer frequency band $\langle R\rangle$ (curve 2) as functions of antenna height h.

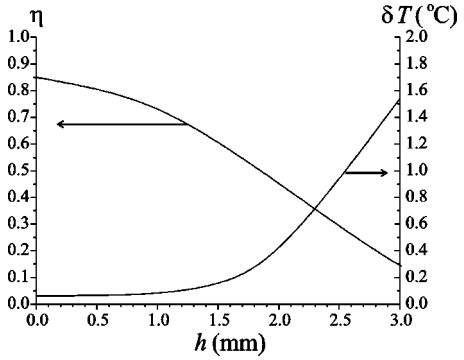

FIG. 7. Antenna efficiency η and sensitivity δT_b in dependence on height h.

function $\langle R(h)\rangle$ was measured independently (see Fig. 6), the formula (6) allows us to determine the dependence $\eta(h)$. The results are presented in Fig. 7, which also shows the function $\delta T_b(h)$.

The decrease in η with growing h in Fig. 7 is conditioned by the following electromagnetic processes in the antenna. When it operates in radiation mode, its efficiency can be represented as

$$\eta = \frac{R_a}{R_a + R_d}, \tag{7}$$

where R_a is the radiation resistance, and R_d is the equivalent resistance of dissipation in the antenna material and in the matching circuit. The resistance $R_a = R_{\rm nf} + R_r$ is determined, primarily, by absorption of the antenna field (mainly near field) in the conducting medium ($R_{\rm nf}$) and, second, by the escaping radiation (R_r). At $h=0$ the relations $R_{\rm nf} \gg R_r$, $R_a > R_d$ are satisfied; hence, the efficiency is quite high ($\eta \approx 0.85$ according to the data in Fig. 7). With an increase in h, the near-field penetration into the absorbing medium is getting weaker, as this field is concentrated near the aperture; so $R_{\rm nf}$ decreases. Thus, at fairly high values of h we obtain the inverse relations $R_{\rm nf} < R_r$, $R_a \ll R_d$, and face the situation which is typical for the ESA radiating into free space [7,8], when $\eta \ll 1$.

It is readily seen from Fig. 7 that, as the height is varied up to some point $h = h_{\max} \approx 2.5$ mm, the fluctuation threshold of sensitivity of the system increases from ~ 0.075 °C (at $h=0$) to ~ 1 °C (at $h = h_{\max}$). Any further deterioration of sensitivity makes it impossible to carry out radiometry measurements at $h > h_{\max}$. It follows from the above that the drop in sensitivity at higher values of h is determined by both the mismatch and degrading efficiency of the antenna, i.e., according to Eq. (6), $\delta T_b(h) = \delta T / \{\eta(h)[1 - \langle R(h)\rangle]\}$, with $\delta T \approx 0.05$ °C being the inherent sensitivity of the radiometer. The near-field effect also accounts for the functions $R(h)$ and $\langle R(h)\rangle$ shown in Figs. 5 and 6. Variation of the height h causes a change in the input impedance of the antenna and, hence, in the antenna-receiver matching conditions. The plateau observed in the dependences $\langle R(h)\rangle$, $\eta(h)$, $\delta T_b(h)$ at $0 < h < 1$ mm in Figs. 6 and 7 is accounted for by a wider working frequency band of the radiometer compared to that of the antenna, as can be seen in Fig. 5. In addition, when the antenna contacts the medium, the latter's surface deflects under the mechanical impact of the antenna near $h=0$. In our measurements the antenna was isolated from the water by a thin polyethylene film on the medium surface, which caused surface deformation at contact.

TABLE I. Antenna parameters.

D (mm)	$\langle R\rangle$	η	$(1-\langle R\rangle)\eta$	$D_{\rm eff}$ (mm)	$d_{\rm eff}$ (mm)
6	0.22	0.59	0.47	4.2	5
20	0.22	0.85	0.67	13	15
52	0.20	0.87	0.70	37	31

As mentioned above, all antennas in our measuring facility have been designed so as to ensure the best match at $h=0$ and $f = f_0 = 970$ MHz. Despite this provision, antenna matching at an initially assigned arbitrary height h is not a problem fundamentally and can be achieved by adjustment of the matching resonator. At the same time, a drop in efficiency with a decrease in size is a common feature of all ESA's. As for the particular characteristics of these antennas in some assigned interval of D/λ variation, they depend on the right choice of antenna design and its adaptability to the test medium. Each of the three antennas used in our facility was similar in its properties to the antenna with $D=20$ mm (see Figs. 5–7). The values for their key parameters when in contact with water ($T=20$ °C, salinity $S=1.8$ g/dm^3, $d_{\rm sk}=39$ mm) are provided in Table I.

The data in Table I point to the applicability of the antennas for near-field radiometry. It should be noted that the monotonically increasing dependence $\eta(D)$ obtained with the three antennas in question meets our expectations, the smallest antenna with $D=6$ mm ($D/\lambda = 0.02$) exhibiting a fairly appreciable decrease in η. At the same time, this record small-size antenna featured a fairly high efficiency parameter $\eta(1-\langle R\rangle) = 0.47$, sufficient for near-field investigations.

IV. EXPERIMENTAL INVESTIGATIONS OF QUASISTATIONARY FIELD

In conformity with the developed theory, the maximum power likely to be received from a heated absorbing medium corresponds to the Planck intensity of thermal radiation. If the receiving antenna is ideal ($R=0$, $\eta=1$), this power depends neither on the antenna position above the radiating surface, nor on its aperture size. In other words, the Rytov effect of a thermal field energy getting higher near a surface due to the quasistationary component is beyond observation by means of an antenna and radiometer. This conclusion, nevertheless, does not imply a total lack of any detectable QF effects, since it is valid only for a temperature-homogeneous medium. The situation is different when a medium has a depth-inhomogeneous temperature profile $T(z)$. We define an average temperature $T_{\rm av}$ in the depth as the temperature of a uniformly heated medium that ensures reception of as much power P as from the medium with $T(z)$

$\neq$ const. Within this definition, T_{av} coincides with the radio brightness temperature T_b in formula (5). Considering that for the microwave range $\Theta(z) \sim T(z)$ generally, we derive from Eq. (2)

$$T_{\mathrm{av}}(D,h) = \int_{-\infty}^{0} dz K(z,D,h) T(z), \tag{8}$$

where $K = K_W + K_Q$. Equation (8) at $T(z) = T_0 = \mathrm{const}$ yields $T_{\mathrm{av}} = T_0$ if we take into account the normalization (A16). In accordance with Eq. (4), the characteristic scale of depth temperature averaging in Eq. (8) is d_{eff}. As shown by the calculations in Fig. 3, the value d_{eff} proves to depend on the receiving antenna parameters D and h, and to be less than the skin depth $[d_{\mathrm{eff}}(D,h) < d_{\mathrm{sk}}]$. If the dielectric constant of the test medium $|\varepsilon| \gg 1$, the characteristic scale for the wave field is d_{sk}. In this case all that distinguishes d_{eff} from d_{sk} should be attributed to the influence of the QF, which clearly follows from Fig. 3. So, when radiation from a temperature-inhomogeneous medium is received by antennas with different parameters D or h, the radiometer-measured power (2) will also be different by virtue of the dependence $T_{\mathrm{av}}(d_{\mathrm{eff}})$. It is this effect that was used in [5,6] for radiometry measurement of a quasistationary field. Water was chosen as the test medium owing to its dielectric constant ε, which can be calculated to a high accuracy from the available temperature and salinity data (see, for example, [17]). Note that for decimeter waves $|\varepsilon| \gg 1$. Knowing the temperature profile $T(z)$ of the radiating medium, one can find the value of d_{eff} from measurements of T_{av}. Even in our first experiments with water varying in degree of salinity [5,6] we found that $d_{\mathrm{eff}} \approx 0.5 d_{\mathrm{sk}}$. The observed effect gave experimental evidence of a quasistationary thermal field.

Most vividly, the QF effect in question manifests itself when the thermal radiation from a nonuniformly heated medium is measured with several antennas greatly differing in the size D. Therefore, in this work we used an antenna facility of our own design, which is shown in Fig. 4. The antenna parameters are given in Table I. We measured the time dynamics of the brightness temperature $T_b(t)$ during heating of the surface of initially homogeneous water $[T(t=0,z) = T_0 = \mathrm{const}]$ with a wire heater. Simultaneous measurements of the water temperature profile dynamics $T(t,z)$ were made with contact sensors. The radiometry system was calibrated against radiation of the same water medium that was uniformly heated to several different temperature levels $T = T_i = \mathrm{const}$ $(i = 1,2,3,\ldots)$. The water salinity in the experiments, S, was 1.8 g/dm^3. The choice of salinity is accounted for by the fact that at this level the dielectric constant of water has a weak dependence on T [5]. In such conditions $\varepsilon \approx \mathrm{const}$ for a temperature-inhomogeneous water medium, which was suggested in the above theory. So, at $S = 1.8$ g/dm^3 our theory should be in best agreement with the experiment.

The measurement results are presented in Fig. 8 for antennas at a height $h = 0$. It is readily seen that the difference in D largely determines the difference in the dependences $T_{\mathrm{av}}(t)$. Larger antenna sizes D correspond to lower values of T_{av} due to the fact that deeper (hence, less heated) layers of the test medium contribute to T_{av}. Figure 8 also shows the

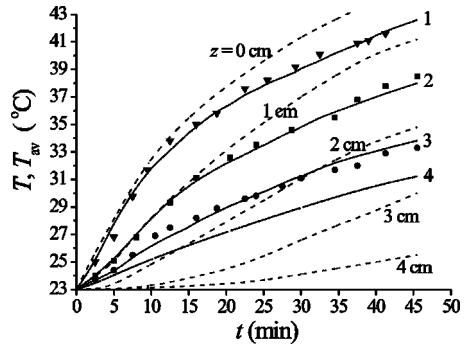

FIG. 8. Brightness temperature dynamics. Symbols, measurements with antennas (1) $D = 6$ mm, (2) $D = 20$ mm, and (3) $D = 52$ mmm. Solid lines, calculations at $D = D_{\mathrm{eff}}$ (curve 4 corresponds to $D \to \infty$). Dashed lines, temperature dynamics at different depths z measured with point-contact sensor.

results of theoretical calculations of the dependences $T_{\mathrm{av}}(t)$. Calculations were made for either antenna by formula (8), using the data from the contact measurements of temperature profiles $T(z,t)$. Note that the best agreement between theory and experiment in Fig. 8 can be ensured by replacing the parameter D in Eq. (8) with its effective value D_{eff}, which turned out to be about 1.5 times smaller than the geometrical size D for all antennas under study (see Table I). This difference can be attributed to the fact that in the expressions for $K(z,D,h)$ [Eqs. (A13) and (A16)] we used the electric field distribution over the antenna aperture in the form $E_a(r) = E_0 \exp(-4r^2/D^2)$. For electrically small antennas the distribution E_a is largely inhomogeneous over the aperture, which results in $D_{\mathrm{eff}} < D$. One may suggest that D_{eff} is the intrinsic parameter of each particular antenna, which does not depend (or is slightly dependent) on the dielectric properties of the test medium and the antenna height above the surface. If so, the values of D_{eff}, once established for each antenna in the facility, can further be used toward near-field diagnostics of media as a parameter of the kernel K in Eq. (A13). This important issue, however, needs to be addressed separately.

Minimal experimental values of T_{av} can be obtained by measuring only the wave component of thermal radiation because of the maximal sounding depth $d_{\mathrm{eff}} \approx d_{\mathrm{sk}}$. Figure 8 shows the dependence $T_{\mathrm{av}}(t)$ for the wave field, which was calculated by formula (8) where the kernel $K(z) = \gamma \exp(\gamma z)$, $\gamma = (4\pi/\lambda)\mathrm{Im}\sqrt{\varepsilon}$ is derived from the general kernel (A13) and (A16) provided $|\varepsilon| \gg 1$, $D/\lambda \gg 1$, $h/\lambda \gg 1$.

The obtained experimental data unambiguously indicate the presence of a near-field component in the thermal radiation of a heated conducting medium. The characteristically QF spatial scale $d_{\mathrm{eff}}(D)$ manifested itself through essential differences in the dependences $T_{\mathrm{av}}(t)$ measured with antennas that varied in aperture size D.

V. NEAR-FIELD RADIOMETRY

As follows from the above, the characteristic property of the quasistationary field is the dependence $d_{\mathrm{eff}}(D,h)$. Experimental values for the effective size of the aperture, D_{eff}, al-

low one to calculate, using formula (4), the effective depth for each antenna in a particular medium. Results of such calculations are presented in Table I for water with salinity $S=1.8\ \mathrm{g/dm^3}$. The obtained dependence $d_{\mathrm{eff}}(D,h=0)$ can be used to acquire data on the subsurface temperature profile $T(z)$. Basically, such measurements are similar to the way the function $d_{\mathrm{sk}}(\lambda)$ is used in the well-known multiwave methods [14,15], since the information on $T(z)$ is contained in the dependence of the average temperature T_{av} on the thickness of the layer in which the received radiation is formed. By simultaneous measurements of T_{av} for several different values of d_{eff}, we can pick up information about the medium temperature at various depth levels and retrieve the profile $T(z)$ by solving Eq. (8). When measuring the QF, one can use the dependence $d_{\mathrm{eff}}(D,h)$, whereas in the wave field measurements only the dependence $d_{\mathrm{sk}}(\lambda)$ should be used. That is, additional opportunities for near-field radiometry lie in the possibility of developing single-wave methods of $T(z)$ retrieval. These methods were first proposed in [18].

The first results of $T(z)$ retrieval from near-field radiometry measurements at a single wavelength were obtained in [5]. However, only two antennas were used in these measurements, the smaller of which had $d_{\mathrm{eff}}\approx 2$ cm ($\sim 0.5 d_{\mathrm{sk}}$). It is known [14] that the minimum set of tools needed for a high enough quality retrieval of simple monotonic profiles $T(z)$ should be able to ensure reception of radiation from three levels of d_{eff} uniformly distributed over the test area. To fill a gap in the experimental data near the boundary, in [5] we made direct measurements of the test medium surface temperature with a contact thermometer. The newly developed antenna facility (see Table I) offered an opportunity for retrieving a $T(z)$ profile without additional measurements of temperature $T(0)$. This can be done since the minimal-size antenna with $d_{\mathrm{eff}}\approx 0.5$ cm($\sim 0.13 d_{\mathrm{sk}}$) gathers information at depth levels close to the surface. In addition, our antenna facility provides a fairly uniform sounding of the area $0<z<d_{\mathrm{sk}}\approx 3.9$ cm, which shows up in Fig. 8 as a considerable difference in the $T_{\mathrm{av}}(t)$ dynamics for different antennas.

Mathematically, the problem of retrieval of the function $T(z)$ from Eq. (8), whose left part has been determined experimentally for several values of the parameter D, is an ill-posed inverse problem [19]. It will take some *a priori* data about the sought-for solution. In our case the monotonically increasing dependences $T(z)$ (at $z<0$) can be approximated by the functions

$$T(z) = T_0 + \frac{1}{a - bz + cz^2}, \tag{9}$$

where $T_0=23\ ^\circ$C is the initial temperature (before the heater was on); $a,b,c>0$ are unknown parameters. Expression (9) should be substituted in Eq. (8). Thus, the retrieval procedure is reduced to finding the parameters a, b, and c by roughly solving the set (8) of three equations. Their left parts contain experimental values of $T_{\mathrm{av}i}$ ($i=1,2,3$) for fixed instants of time t. Approximation of Eq. (9) serves as *a priori* information on $T(z)$ because the function (9) is monotonically increasing for all values of the parameters a, b, and c. The use of three unknown parameters in the expansion is caused by the availability of experimental data obtained with three antennas.

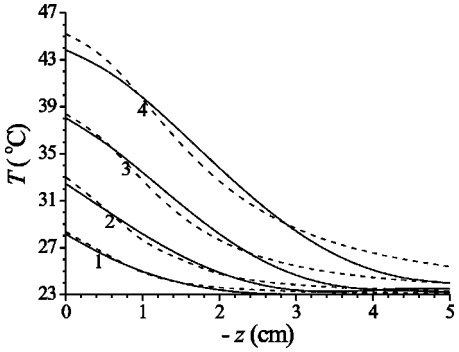

FIG. 9. Dashed lines, temperature profiles retrieved by measured data of $T_b(t,D)$ in Fig. 8. Solid lines, results of contact measurements. Curve 1 corresponds to $t=5$ min after the heater was on; 2, 10 min; 3, 20 min; 4, 40 min.

Figure 9 exemplifies retrieval of $T(z)$ profiles at some instants of time after the heater was turned on. It also shows the data obtained through contact measurements of temperature at the same moments. One can see that the resulting profiles agree to an accuracy of about 10% with the value of $\Delta T(z)=T(z)-T_0$ (or better than 1.5 °C) which corresponds to the limits of our measurements error estimated at $\sim 1\ ^\circ$C for the maximal value of $\Delta T(z)$.

VI. CONCLUSION

In this work we report the results of our investigations into the quasistationary field of thermal emission from absorbing media. A theory of QF measurement is developed, which shows that the effect of QF enhancement on the surface of a radiating medium, predicted by Rytov, is beyond radiometry capabilities. It manifests itself only through the redistribution of energy between the wave and the quasistationary components. The sum of the components is constant and it corresponds to the Planck intensity. The contribution of the QF in the measured power dominates if the receiving antenna parameters are $D/\lambda \ll 1$, $h/\lambda \ll 1$. There is, however, another effect that can be of practical use for QF detection. Essentially, it is the QF-related space scale d_{eff} that depends on the antenna parameters D and h; note that $d_{\mathrm{eff}}(D,h)<d_{\mathrm{sk}}$. Experimental study of this effect is possible with antennas of small electrical size. Our investigations have shown the properties of such antennas to be adequate for detection of QF effects. Measurements of the radiation from nonuniformly heated water carried out with antennas of varied sizes allowed us to register the above effect. It indicates without ambiguity the existence of a quasistationary component in the thermal field. Advances in near-field radiometry open up additional opportunities for the subsurface diagnostics, as variation of antenna height h or size D enables one to examine the medium at different levels of depth. In particular, we succeeded in retrieving a temperature depth profile experimentally. The QF measurements were carried out at a single wavelength through the use of antennas of various sizes.

The challenging issue that remains unsolved so far is whether near-field radio thermal microscopy is feasible. At present, near-field microscopy in the microwave range involves only active systems [20]. Some of them operate at $D/\lambda \approx 10^{-5}$ and feature submicrometer resolution [21], since it is the aperture size D that space resolution depends on. A distinguishing feature of thermal emission detectors is that their antennas have to show high efficiency and good matching within a wide band of reception. For example, an antenna having $\eta=0.3$ and $R=0.3$ will make a detector with sensitivity of just 20% of the radiometer sensitivity. The antennas of our design provide high enough sensitivity at $D/\lambda > 10^{-2}$. Reduction of the aperture scales to $D/\lambda < 10^{-4}$ will apparently require some new antenna design to ensure the same level of sensitivity. Quite likely, higher efficiency of near-field antennas can be achieved through the use of superconducting materials, as is done in the case of electrically small antennas radiating in free space [8–10]. It should be noted, however, that in pursuing superhigh resolution of a near-field microscope we may end up losing one prime advantage of electromagnetic fields in the microwave range, essentially, their relatively high penetrability in many media (biological tissues, water, soils, etc.). As shown in this work, there is a definite relation between the aperture size D and the effective probing depth d_{eff}, the latter decreasing with a smaller D/λ.

ACKNOWLEDGMENTS

The authors are grateful to G. M. Altshuller, S. A. Basov, and S. V. Ponomarev for their assistance in manufacturing the antennas and the measuring facility. The work was supported by the Russian Foundation for Basic Research, Grant No. 03-02-16086.

APPENDIX: THERMAL RADIATION POWER RECEIVED BY NEAR-FIELD ANTENNA

The principle of near-field radiometry is shown schematically in Fig. 1. The aperture of a receiving antenna is positioned in vacuum at a height h above the surface of a heated medium (it is also possible that $h=0$). The signal to be measured is proportional to the value of the mean energy flow P in some cross section h_w of the receiving circuit waveguide. To ensure system excitation without reflection, a matching device is used with the input impedance Z_{in} satisfying the conditions $\text{Im}\, Z_{\text{in}}=0$, $\text{Re}\, Z_{\text{in}}=Z_w$, where Z_w is the wave impedance of the corresponding waveguide mode.

Thermal radiation of a medium is generated by fluctuation current $\mathbf{j}(\mathbf{r},z)$ which is set by the correlation function (1). The current $\mathbf{j}$ induces electric and magnetic fields in the cross section h_w of the receiving circuit waveguide, whose $\mathbf{E}(\mathbf{r})$ and $\mathbf{H}(\mathbf{r})$ components are expressed in terms of the eigenfunctions of the waveguide mode, $\vec{\varphi}_e(\mathbf{r})$ and $\vec{\varphi}_m(\mathbf{r})$ (the vectors $\vec{\varphi}_e$ and $\vec{\varphi}_m$ are orthogonal):

$$\mathbf{E}(\mathbf{r}) = E_{\max}\vec{\varphi}_e(\mathbf{r}),$$

$$\mathbf{H}(\mathbf{r}) = H_{\max}\vec{\varphi}_m(\mathbf{r}), \tag{A1}$$

where $E_{\max}$, $H_{\max}$ are the maximum amplitudes of the fields. The eigenfunctions are normalized: $\varphi_e^{\max}=\varphi_m^{\max}=1$. The vector of the thermal radiation energy flow, $\mathbf{S}=(c/8\pi)\text{Re}[\mathbf{E}\times\mathbf{H}^*]$ (c is the speed of light) is directed from the antenna to the receiver.

Let us consider an auxiliary problem on antenna radiation into an absorbing medium, which is excited by an electromagnetic wave propagating in the receiving waveguide toward the antenna. The auxiliary wave fields in the waveguide cross section h_w have a structure like Eq. (A1) with amplitudes $E^w_{\max}$ and $H^w_{\max}$. The energy flow of such a wave is opposite to $\mathbf{S}$. Following the general rule of treating radiation problems, we consider a surface electric current $\vec{\xi}(\mathbf{r})$ in the cross section h_w. This current is a source for the antenna radiation field. It has a spatial structure that is similar to the structure of the magnetic field in the waveguide, and is directed orthogonally to $\mathbf{H}^w$ at each point:

$$\vec{\xi}(\mathbf{r}) = -\frac{c}{4\pi}H^w_{\max}[\vec{\varphi}_m(\mathbf{r})\mathbf{z}^0], \tag{A2}$$

where $\mathbf{z}^0$ is the unit vector of the z axis in Fig. 1. The current $\vec{\xi}$ induces an electric field $\mathbf{E}_m(\mathbf{r},z)$ in the medium and radiated fields $\mathbf{E}_r(\mathbf{r},z)$, $\mathbf{H}_r(\mathbf{r},z)$ in vacuum.

We now use the reciprocity theorem for currents $\mathbf{j}$, $\vec{\xi}$ and fields $\mathbf{E}$, $\mathbf{E}_m$ induced by these currents:

$$\int_V \mathbf{j}(\mathbf{r},z)\mathbf{E}_m(\mathbf{r},z)dV = \frac{c}{4\pi}H^w_{\max}E_{\max}S_{\text{eff}}, \tag{A3}$$

where $S_{\text{eff}}=\int_S \varphi_e(\mathbf{r})\varphi_m(\mathbf{r})d^2r$ is the effective cross-sectional area of the waveguide. The mean energy flow of the thermal radiation in the waveguide is defined as

$$P = \frac{c}{8\pi}\langle|E_{\max}|^2\rangle S_{\text{eff}}\frac{1}{Z_w}, \tag{A4}$$

where the wave impedance of the mode $Z_w=E_{\max}/H_{\max}$.

Substitution of the field $E_{\max}$ from Eq. (A3) into Eq. (A4) with allowance for Eq. (1) yields

$$P = \frac{\omega\varepsilon_2}{2\pi c|H^w_{\max}|^2 S_{\text{eff}}}\frac{1}{Z_w}\int_{-\infty}^{0} dz\Theta(z)\int\int d^2r|\mathbf{E}_m(\mathbf{r},z,h)|^2. \tag{A5}$$

Thus, determination of the energy flow of thermal radiation, P, is reduced to the problem of auxiliary wave absorption in the conducting medium. We find a solution of this problem through the use of the energy conservation law for the energy flow of an auxiliary wave in the waveguide,

$$P_w = \frac{c}{8\pi}Z_w|H^w_{\max}|^2 S_{\text{eff}}.$$

In the case of reflectionless excitation the value of P_w is partly absorbed in the antenna material (P_a), partly dissipated in the test medium (P_m), with the remaining part (P_r) being reradiated into free space, i.e., $P_w=P_a+P_r+P_m$. We assume that $P_a \ll (P_m+P_r)$, which means that the antenna efficiency $\eta=(P_m+P_r)/P_w \approx 1$.

The powers P_m and P_r are defined by the relations

$$P_m = \frac{\omega\varepsilon_2}{8\pi}\int_V dz d^2r |\mathbf{E}_m(\mathbf{r},z,h)|^2, \tag{A6}$$

$$P_r = \frac{c}{8\pi}\int_S d^2r\ \mathrm{Re}[\mathbf{E}_r(\mathbf{r},z)\mathbf{H}_r^*(\mathbf{r},z)]_z. \tag{A7}$$

The integration region in Eq. (A6) covers the whole volume of the absorbing medium ($z<0$). In Eq. (A7) this region is a plane parallel to the medium surface ($z=0$) and located at an arbitrary height above the antenna aperture $z>h$.

Taking account of the condition $P_w=P_m+P_r$, from Eq. (A5) we derive

$$P = \frac{1}{2\pi}\frac{\int_{-\infty}^{0} dz\Theta(z)\int\int d^2r|\mathbf{E}_m(\mathbf{r},z,h)|^2}{\int dz d^2r|\mathbf{E}_m(\mathbf{r},z,h)|^2 + (c/\omega\varepsilon_2)\int d^2r\ \mathrm{Re}[\mathbf{E}_r(\mathbf{r},z)\mathbf{H}_r^*(\mathbf{r},z)]_z}, \tag{A8}$$

which is essentially the generalized Kirchhoff law extended to the conditions of the problem under study.

The fields $\mathbf{E}_m$, $\mathbf{E}_r(\mathbf{r},z)$, and $\mathbf{H}_r(\mathbf{r},z)$ in Eqs. (A6) and (A7) are expressed in terms of the distribution of the electric field $\mathbf{E}_a(\mathbf{r})$ and magnetic field $\mathbf{H}_a(\mathbf{r})$ over the receiving antenna aperture. This distribution is generally specified for every particular antenna design. In this case, the fields can be found by using the well-known Green function G of a half space with radiation sources as point electric or magnetic dipoles placed over the antenna aperture:

$$\mathbf{G}^{e,m}(\mathbf{r}-\mathbf{r}_1,z,h) = \mathbf{G}^{ee,me}(\mathbf{r}-\mathbf{r}_1,z,h) + \mathbf{G}^{em,mm}(\mathbf{r}-\mathbf{r}_1,z,h), \tag{A9}$$

where $\mathbf{r},z$ are the coordinates in the surrounding space, and $\mathbf{r}_1$ are the coordinates in the aperture of the antenna. We assume also that $E_a(\mathbf{r}_1)=H_a(\mathbf{r}_1)$, with vectors $\mathbf{E}_a,\mathbf{H}_a$, being aligned with the axes y,x, respectively. It is convenient to express $\mathbf{G}=G_1\mathbf{x}^0+G_2\mathbf{y}^0+G_3\mathbf{z}^0$ in terms of the corresponding Fourier transforms along the transverse coordinates:

$$\int\int d^2r|\mathbf{E}_m(\mathbf{r},z,h)|^2 = \frac{4c^2}{(4\pi)^4}\int\int d^2\kappa\sum_{i=1}^{3}|G_i^e(\vec{\kappa},z,h)|^2|E_a(\vec{\kappa})|^2, \tag{A10}$$

$$\int\int d^2r\ \mathrm{Re}[\mathbf{E}_r(\mathbf{r},z)\mathbf{H}_r^*(\mathbf{r},z)]_z = \frac{4c^2}{(4\pi)^4}\int\int d^2\kappa\ \mathrm{Re}[G_1^e(\vec{\kappa},z)G_2^{m*}(\vec{\kappa},z) - G_2^e(\vec{\kappa},z)G_1^{m*}(\vec{\kappa},z)]_z|E_a(\vec{\kappa})|^2. \tag{A11}$$

The form of the $\mathbf{G}^{e,m}(\vec{\kappa},z,h)$ functions for the problem in question is given in [22]. Therefore, we here provide only the ultimate result to be obtained through substitution of Eqs. (A10) and (A11) in Eq. (A8):

$$P = \frac{1}{2\pi}\frac{\int_{-\infty}^{0} dz\Theta(z)\tilde{K}(z,h)}{\int_{-\infty}^{0} dz\tilde{K}(z,h) + K_r}, \tag{A12}$$

where

$$\tilde{K}(z,h) = \int\int d^2\kappa\left[\frac{\kappa_y^2}{\kappa^2}|T_E|^2 + \frac{\kappa_x^2}{\kappa^2}|T_H|^2|n_\parallel|^2\right]\left|\frac{k_0+\sqrt{k_0^2-\kappa^2}}{\sqrt{k_0^2-\kappa^2}}\right|^2 \times \exp(2\,\mathrm{Im}\sqrt{\varepsilon k_0^2-\kappa^2}z) \times \begin{Bmatrix} 1, & \kappa\leqslant k_0 \\ \exp(-2\sqrt{\kappa^2-k_0^2}h), & \kappa>k_0 \end{Bmatrix} \times |E_a(\vec{\kappa})|^2, \tag{A13}$$

$$K_r = \int\int d^2\kappa\left[\frac{\kappa_y^2}{\kappa^2}|R_E|^2 + \frac{\kappa_x^2}{\kappa^2}|R_H|^2|n_\parallel|^2\right] \times \left|\frac{k_0+\sqrt{k_0^2-\kappa^2}}{\sqrt{k_0^2-\kappa^2}}\right|^2|E_a(\vec{\kappa})|^2, \tag{A14}$$

where $k_0=2\pi/\lambda$ is the wave number in vacuum,

$$T_E = \frac{2\sqrt{k_0^2-\kappa^2}}{\sqrt{k_0^2-\kappa^2}+\sqrt{\varepsilon k_0^2-\kappa^2}},\ T_H = \frac{2\varepsilon\sqrt{k_0^2-\kappa^2}}{\varepsilon\sqrt{k_0^2-\kappa^2}+\sqrt{\varepsilon k_0^2-\kappa^2}}$$

are the Fresnel transmission coefficient for waves of E and H polarization, $R_{E,H}=T_{TE,H}-1$ are the corresponding reflection coefficients, and $|n_\parallel|^2=(|\sqrt{\varepsilon k^2-\kappa^2}|^2+\kappa^2)/k^2|\varepsilon|^2$.

It is important to note that Eq. (A14) was obtained considering the condition that the antenna radiation pattern has only loops turned toward the medium. In other words, we suppose the radiation P_r to be formed only by the reflection from the surface of the medium under study. A low level of back loops is quite typical for microstrip antennas similar to those shown in Fig. 4.

In accordance with Eq. (A12) the maximal power P can be received when $P_r \ll P_m$. This situation takes place if the

antenna with $D/\lambda \ll 1$ is located at $h \ll \lambda$ over the conductive medium. For $h > \lambda$ we usually have the opposite relation: $P_r \sim P_m$ (water, biological tissues) or $P_r \gg P_m$ (metals). In Eq. (A12) we can neglect K_r if the reflected power P_r is directed back to the absorbing medium. In practice it can be done by placing the antenna under an ideal-reflecting plane screen. This method was applied for radiometry measurements in [14,15]. Assuming $K_r = 0$, from Eq. (A12) we obtain

$$P = \frac{1}{2\pi}\int_{-\infty}^{0} dz\Theta(z)K(z,h), \tag{A15}$$

where

$$K(z,h) = \frac{\tilde{K}(z,h)}{\int_{-\infty}^{0} dz\tilde{K}(z,h)}. \tag{A16}$$

The formula (A15) describes the contribution of the wave and the quasistationary fields in the antenna-received radiation. The wave field corresponds to the integration region $\kappa \leq k_0$ in Eq. (A13), and the quasistationary field to the region $\kappa > k_0$. Hence, the kernel K of Eq. (A15) can be represented as $K = K_W + K_Q$, which will lead us from Eq. (A15) to Eq. (2).

When the QF component in Eq. (A13) is negligible (i.e., $D/\lambda \gg 1$ or $h/\lambda \gg 1$), we may turn to angular variables $\kappa_x = k_0 \sin\theta\cos\phi$, $\kappa_y = k_0 \sin\theta\sin\phi$, since $\kappa = \sqrt{\kappa_x^2 + \kappa_y^2} \leq k_0$. This substitution leads from Eq. (A12) to the well-known result of wave theory for the thermal radiation of a half space, receivable by an antenna:

$$P_W = \lambda^2 \int_0^{2\pi}\int_0^{\pi/2} d\phi d\theta \sin\theta I(\theta,\phi)\Phi(\theta,\phi), \tag{A17}$$

where

$$I(\theta,\phi) = \frac{1}{2\pi\lambda^2}\int_{-\infty}^{0} dz\Theta(z)\gamma(\theta)\exp[\gamma(\theta)z] \times\{\cos^2\phi[1 - |R_E(\theta)|^2] + \sin^2\phi[1 - |R_H(\theta)|^2]\}$$

is the ray intensity (or brightness) of radiation from a nonuniformly heated half space. It can also be derived from the radiation transfer equation by assuming $\gamma(\theta) = 2k_0 \operatorname{Im}\sqrt{\varepsilon - \sin^2\theta}$ is the medium absorption coefficient. The normalized directivity pattern $\Phi(\theta,\phi)$ is expressed in terms of the field angular spectrum on the receiving antenna aperture $E_a(\theta,\phi) = \int d^2 r E_a(\mathbf{r})\exp[ik_0 \sin\theta(x\cos\phi + y\sin\phi)]$:

$$\Phi(\theta,\phi) = \frac{(1+\cos\theta)^2|E_a(\theta,\phi)|^2}{\int_0^{2\pi}\int_0^{\pi/2} d\phi d\theta \sin\theta(1+\cos\theta)^2|E_a(\theta,\phi)|^2}. \tag{A18}$$

It is evident that for $\Theta(z) = \Theta = \text{const}$ from Eq. (A17) we obtain $P_W < P_0$ because $R_{E,H} \neq 0$ in contrast to Eqs. (A15) and (A16), where $P_W \to P_0$ for $h/\lambda \gg 1$ or $D/\lambda \gg 1$.

As known, the near-field component P_Q in Eq. (2) is not described by the wave theory, although it also contributes in the total measurable power (A15).

For comparison with the obtained solution (A15) and (A16), let us consider the mean energy density w of a thermal field above the absorbing half-space surface when it is not transformed by receiving system. Using the theory developed in [2] for half-space radiation and the spectral representation of the Green function used in this work, we readily have

$$w(h) = \frac{\omega\varepsilon_2}{(2\pi)^3 c^2}\int_{-\infty}^{0} dz\Theta(z)\tilde{K}_{\text{free}}(z,h). \tag{A19}$$

The kernel $\tilde{K}_{\text{free}}(z,h)$ of Eq. (A19) consists of two parts corresponding to the wave and the quasistationary thermal fields. It is described by formula (A13) ignoring the multiplier $|E_a(\vec{\kappa})|^2$. The expression (A19) is one way of representing the solution to the problem on the thermal field of a half space obtained by Rytov [2].

[1] S. M. Rytov, *Theory of Electrical Fluctuations and Heat Emission* (Akademii Nauk SSSR, Moscow, 1953).

[2] S. M. Rytov, Yu. A. Kravtsov, and V. I. Tatarskii, *Principles of Statistical Radiophysics* (Springer-Verlag, Berlin, 1987).

[3] A. A. Andronov and Yu. A. Ryzhov, Usp. Fiz. Nauk **126**, 323 (1978).

[4] I. Dorofeyev, H. Fuchs, and J. Jersch, Phys. Rev. E **65**, 026610 (2002).

[5] K. P. Gaikovich, A. N. Reznik, V. L. Vaks, and N. V. Yurasova, Phys. Rev. Lett. **88**, 104302 (2002).

[6] K. P. Gaikovich and A. N. Reznik, JETP Lett. **72**, 792 (2000).

[7] R. C. Hancen, IEEE Trans. Microwave Theory Tech. **39**, 1508 (1991).

[8] A. Yu. Klimov *et al.*, Supercond., Phys. Chem. Technol. **6**, 542 (1993).

[9] V. I. Abramov, A. Yu. Klimov, A. N. Reznik, and B. B. Tagunov, Tech. Phys. Lett. **20**, 792 (1994).

[10] R. K. Belov *et al.*, IEEE Trans. Appl. Supercond. **5**, 2579 (1995).

[11] F. Bardati and D. Solimini, Radio Sci. **18**, 1393 (1983).

[12] B. Bocquet *et al.*, IEEE Trans. Microwave Theory Tech. **38**, 791 (1990).

[13] K. I. Carr, IEEE Trans. Microwave Theory Tech. **37**, 1862 (1989).

[14] K. P. Gaikovich, A. N. Reznik, M. I. Sumin, and R. V. Troitskii, Izv. Akad. Nauk SSSR, Ser. Fiz. Atmos. Okeana (in Russian) 23, 569 (1987).

[15] K. P. Gaikovich, A. N. Reznik, and R. V. Troitskii, Radiophys. Quantum Electron. **32**, 987 (1989).

[16] V. L. Vaks, K. P. Gaikovich, and A. N. Reznik, Radiophys.

Quantum Electron. **45**, 7 (2002).
[17] L. A. Klein and C. T. Swift, IEEE Trans. Antennas Propag. **25**, 104 (1977).
[18] A. N. Reznik, Radiophys. Quantum Electron. **34**, 512 (1991).
[19] A. N. Tikhonov and V. Y. Arsenin, *Solutions of Ill-Posed Problems* (Wiley, New York, 1977).
[20] B. T. Rosner and D. W. van der Weide, Rev. Sci. Instrum. **73**, 2505 (2002).
[21] I. Takeuchi *et al.*, Appl. Phys. Lett. **14**, 2026 (1997).
[22] E. L. Feinberg. *Wave Propagation Over the Ground* (Akademii Nauk SSSR, Moscow, 1961).